
REVERSE: Reinforcing Evidence Verification and Search for Agentic Image geo-localization

Yong Li^{1,2,*} Furong Jia^{1,*} Dacheng Yin^{3,†} Kang Rong³
Fengyun Rao³ Jing LYU³ Fan Zhang^{2,†}

¹Peking University

²The Hong Kong University of Science and Technology

³WeChat Vision, Tencent Inc

Abstract

Image geo-localization aims to determine where a photograph was taken, a task that often requires more than recognizing visible landmarks. Human experts typically solve it through an iterative workflow: they inspect informative regions, form location hypotheses, seek external evidence, and revise their judgments as new clues appear. Existing methods only partially capture this process: direct prediction methods bypass evidence acquisition altogether, while retrieval-augmented methods introduce external evidence but usually provide limited supervision on the intermediate decisions of where to search, how to query, and how to filter noisy results. We present REVERSE, a framework that reinforces the interplay between evidence search and verification to enable multi-turn agentic reasoning. REVERSE teaches three intermediate decisions: where to look, what to query, and what evidence to trust. To support this, we construct tool-grounded trajectories with annotated region selections, search observations, and geo-informative evidence labels, and introduce process rewards for visual grounding, query utility, and evidence discrimination. An offline search cache makes retrieval observations stable and reusable during reinforcement learning, enabling dense supervision over noisy search results. With a 4B model, REVERSE outperforms strong retrieval-augmented baselines and rivals substantially larger models on Im2GPS3k and YFCC4k. Code is available at <https://github.com/yong1lee/REVERSE>.

1 Introduction

Image geo-localization estimates the geographic location of a photograph from its visual content [1, 2], with applications in navigation, urban analysis, and remote sensing. Prior methods either partition the Earth into cells and train classifiers [3–5], match the image against geo-tagged databases [6–8], or use large vision-language models to reason toward coordinate predictions [9–11]. All commit to a single prediction without querying or verifying external evidence, so performance is bounded by what the model already knows when the scene contains unfamiliar landmarks or ambiguous visual cues.

Recent agentic methods address this by allowing models to interact with tools across multiple turns [12–15], but tool access alone does not guarantee reliable geo-localization. Figure 1(A) shows two representative failures: a model that crops the wrong region submits it to image search and follows misleading results to a wrong prediction; a model that retrieves the right candidate cannot separate it from distractors and again predicts incorrectly. Both failures reveal that agentic geo-localization hinges on three intermediate decisions: *where to look* (identifying which visual cues

*Equal contribution.

†Corresponding author.

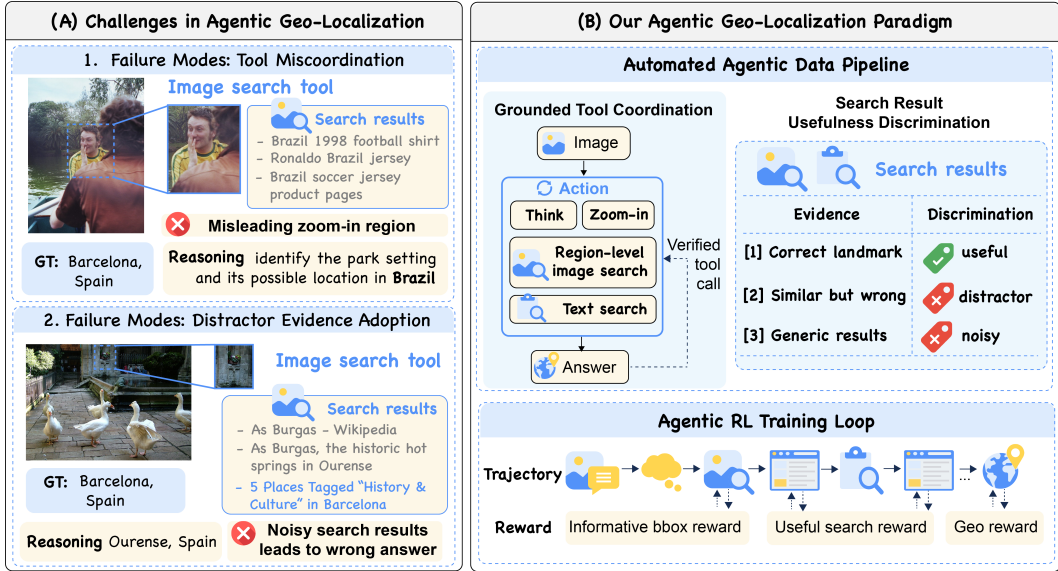


Figure 1: (A) Agentic geo-localization fails when a model crops the wrong region and follows misleading results, or retrieves the right candidate but cannot filter distractors. (B) REVERSE fixes both: spatial supervision grounds region selection, evidence labels annotate search results, and process rewards train the model via agentic RL.

are geographically informative), *how to query* (formulating a query that retrieves relevant external evidence), and *what to trust* (discriminating genuine evidence from visually similar distractors). Yet none receives explicit supervision under standard final-coordinate training, and no existing method addresses all three.

We present REVERSE (**R**einforcing **E**vidence **V**erification and **S**earch for Agentic Image Geo-localization), which treats these three decisions as explicit optimization targets. If the model must make observable choices at each step (*where to look*, *how to query*, *what to trust*), each choice can be supervised directly. We build a data pipeline that generates teacher trajectories annotated with region selections and per-result evidence labels, providing ground truth where final-coordinate training has none. We design process rewards for each decision and train offline against a pre-built search cache, so the full agentic reasoning loop is directly optimizable.

We evaluate on Im2GPS3k [16] and YFCC4k [17]. With a 4B model, REVERSE reaches 48.3% accuracy at 25 km on Im2GPS3k, outperforming all retrieval-augmented baselines and matching models more than an order of magnitude larger.

In summary, our contributions are threefold.

- We introduce REVERSE, an agentic image geo-localization framework that reinforces evidence search and verification by jointly aligning tool use with spatial region selection, query formulation, and evidence discrimination across multi-turn reasoning chains.
- We build a tool-grounded data generation pipeline that annotates not only final locations, but also region selections, search observations, and geo-informative evidence labels, enabling supervision over where to search, how to query, and what to trust during reasoning.
- We perform agentic reinforcement learning with a composite reward that combines geographical accuracy, format compliance, tool-use quality, and evidence discrimination, allowing a 4B vision-language model to achieve strong performance on geo-localization benchmarks.

2 Related work

2.1 Image geo-localization

Image geo-localization aims to predict the geographic location of a given image and has broad applications in urban analysis, navigation, remote sensing, and geospatial data mining. It has long been studied as a visual recognition problem, with early methods predicting locations through geographic partitioning, hierarchical classification, or retrieval from geo-tagged image databases [3–5, 16]. Later work improves visual-location modeling with stronger backbones, and contrastive image-location alignment [18, 19, 6, 7]. With the emergence of large vision-language models, recent methods increasingly cast geo-localization as a language-mediated reasoning problem, where visual cues can be described, compared, retrieved, and verified using external knowledge. Retrieval-augmented approaches ground predictions with candidate images, geographic databases, or web evidence [8, 9, 20], showing the value of external database beyond closed-book visual prediction. Beyond retrieval, recent LVLM-based methods further strengthen geographic reasoning through reinforcement learning [21, 10, 11]. More recent agentic methods further explore multi-agent collaboration, map-based interaction, reinforced geographic reasoning, and tool-augmented hypothesis verification [14, 13, 12]. These works demonstrate the value of external evidence and multi-step reasoning for image geo-localization, but the search and verification process itself is rarely an explicit optimization target.

2.2 Multimodal agentic reasoning.

Large vision-language models are increasingly extended from static perception to interactive reasoning with external tools. Early tool-augmented systems connect foundation models with visual modules, program execution, web search, and structured environments, showing that complex multimodal tasks often require iterative perception, action, and evidence aggregation [22–26]. More recent work further internalizes such behaviors through cold start trajectories and reinforcement learning, enabling models to decide when to invoke tools, how to combine visual operations with textual search [27–32]. These studies indicate a broader shift from static multimodal understanding toward long-horizon evidence acquisition. However, most existing settings focus on general visual question answering or open-domain research tasks, where evidence only needs to support a textual answer. Image geo-localization requires spatially and geographically discriminative evidence for coordinate prediction, making reliable search and verification particularly challenging.

3 Method

REVERSE recasts image geo-localization as an iterative process of visual inspection, evidence retrieval, and hypothesis verification. As illustrated in Figure 1, effective agentic geo-localization requires the model to make three intermediate decisions: *where to look*, *how to query*, and *what to trust*. Our method is organized around three corresponding components: an agentic geo-localization framework that defines tool-mediated reasoning (Section 3.1), a data generation pipeline that constructs trajectories and evidence labels for these decisions (Section 3.2), and a three-stage post-training procedure (SFT, Agentic Cold Start, and Agentic RL) that converts these signals into model behavior (Section 3.3).

3.1 Agentic geo-localization framework

Expert human geo-localization is rarely a single visual matching step. A human expert first inspects potentially informative visual cues, forms tentative geographic hypotheses, searches for external evidence, and then revises the hypothesis based on the reliability of the retrieved clues. We formulate image geo-localization as a multi-turn multimodal reasoning problem that follows the same cognitive loop. Given a query image I , the agent produces a trajectory

$$\tau = (I, a_1, o_1, \dots, a_T, o_T, \hat{y}), \tag{1}$$

where a_t denotes the action at turn t , o_t denotes the corresponding observation, and \hat{y} is the final predicted location. At each turn, the agent first generates a <think> trace and then either calls one tool or outputs a final answer. We restrict each response to at most one tool call so that the effect of each action can be attributed clearly during training. After a bounded number of turns, the agent

must produce the final prediction in the format

`<answer> country, city, latitude, longitude </answer>`. (2)

A central design choice is the `<useful>` tag. Search tools usually return a ranked list of results, only some of which provide reliable geographic evidence. After receiving image search or text search results, the agent is required to output a tag such as

`<useful>[1, 3]</useful>`,

where the indices refer to retrieved results that the model judges to be geo-informative. An empty tag, `<useful>[]</useful>`, indicates that none of the returned results should be trusted. This explicit evidence selection interface makes the model’s judgment observable and allows the reward to evaluate whether the agent has learned *what to trust*. The agent is equipped with three tools.

Zoom tool. The zoom tool takes a normalized bounding box $b = (x_1, y_1, x_2, y_2)$ and returns a cropped, resized view of the selected region. It helps the agent inspect fine-grained visual cues that may be too small or ambiguous in the full image, such as signs, road markings, inscriptions, architectural details, and distant landmarks. In our framework, zoom is not a generic enhancement operation. It is an explicit action for selecting potentially geo-informative regions.

Image search tool. The image search tool performs region-level reverse image search. Instead of submitting the full image, the agent selects a bounding box and searches the cropped region. This design is important because full-image retrieval can be dominated by salient but geographically irrelevant content, while a carefully selected region can expose distinctive landmarks, storefronts, signs, or local visual patterns. The tool returns a ranked list of results with titles, source domains, and links, which the agent must then filter using the `<useful>` tag.

Text search tool. The text search tool accepts a natural-language query and returns web snippets. It complements visual search by verifying candidate place names, landmarks, addresses, or textual clues inferred from previous observations. Together, the three tools cover the full reasoning loop: where to look in the image, how to query external sources, and what retrieved evidence to trust.

3.2 Data generation pipeline

Training an agent for geo-localization requires more than final coordinate labels. The environment must expose learnable signals for the full cognitive loop: *where to look* through precise crop selection, *how to query* through text and image search actions, and *what to trust* through evidence discrimination. We construct such an environment using Kimi-K2.6 as a teacher model (Figure 2).

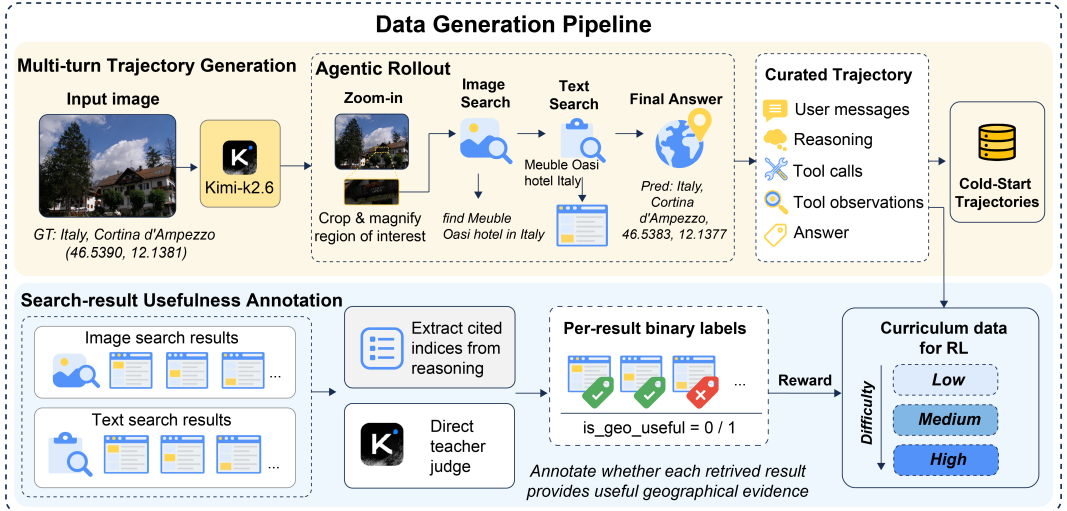


Figure 2: **Data generation pipeline.** Kimi-K2.6 generates multi-turn geo-localization trajectories over MP-16 Pro images using live search APIs. Trajectories undergo quality filtering, geo-informative label annotation, and bounding box re-annotation to correct full-image crops. The resulting dense annotations populate an offline cache that supports API-free RL training.

Trajectory generation and filtering. We source training images from the MP-16 Pro dataset and prompt Kimi-K2.6 to solve each image using the same agentic tool interface as the student model. The teacher produces multi-turn trajectories containing reasoning traces, zoom calls, region-level image search calls, text search queries, `<useful>` tags, and final answers. We filter out inaccessible images, failed teacher trajectories whose final prediction is too far from the ground truth, tool-free trajectories, and trajectories requiring excessive intervention. This yields a set of valid teacher trajectories that provide demonstrations of how visual inspection, search, and verification can be coordinated.

Search result and crop region annotation. Raw teacher outputs leave two annotation gaps that we close with a second pass using Kimi-K2.6. First, evidence labels are incomplete: for each cached image search call, the teacher judges whether each returned result provides concrete geographic evidence for the target image, using any result indices already cited in the reasoning trace as initial signals and evaluating the remaining candidates directly. This produces per-result binary labels (`is_geo_useful`) that later drive the evidence discrimination reward. Second, a large fraction of image search calls use full-image bounding boxes, which weaken the *where to look* signal because a model can achieve high spatial overlap without localizing any specific cue. We prompt the teacher to redraw these as tighter crops around the most geo-informative region, keeping the original search results intact. The corrected boxes serve as spatial targets for reward computation.

Offline search cache. We materialize all image search and text search observations into offline caches. Each image search entry stores the annotated bounding box, geo-informative positive results, and non-informative negatives from the same ranked list—the latter are deliberately hard since they come from the same query and are often visually or semantically related to the true location. During RL rollout, model-generated image-search boxes are matched to cached entries by IoU; text queries are matched by token-level Jaccard similarity. This keeps retrieval observations stable and reusable across training steps while preserving the noise structure of real search results.

Curriculum construction. The evidence discrimination reward requires every search call in a trajectory to carry usefulness labels. We retain trajectories meeting this condition, plus any that make no search calls at all, to form the full-curriculum set. A separate easy-curriculum subset restricts further to examples where the teacher’s localization error is small. RL begins on this easier subset to stabilize tool-use behavior, then continues on the full-curriculum set for harder, more diverse samples.

3.3 Three-stage training pipeline

As illustrated in Figure 3, REVERSE trains in three stages.

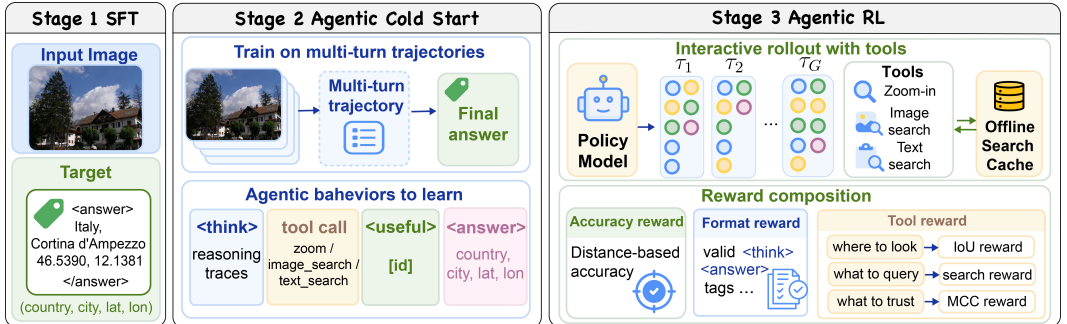


Figure 3: **REVERSE training pipeline.** The model first learns direct image geo-localization through SFT, then acquires multi-turn tool-use behavior from cold start trajectories, and finally undergoes agentic RL with offline search observations. The reward combines geographical accuracy, format compliance, and process-level signals for where to look, how to query, and what to trust.

Stage 1: SFT. We fine-tune Qwen3-VL-4B-Instruct [33] on 4M geo-tagged images from MP16-Pro [9], training the model to output coordinates directly from the image with no tools or reasoning chain, the goal is to build a strong geographic memory before introducing any agentic behavior.

$$\mathcal{L}_{\text{geo}} = - \sum_t \log p_{\theta}(a_t | I). \tag{3}$$

Stage 2: Agentic Cold Start. To initialize the correct interaction protocol, we fine-tune Qwen3-VL-4B-Instruct on 4,427 curated teacher trajectories using standard autoregressive modeling:

$$\mathcal{L}_{\text{SFT}} = - \sum_t \log p_{\theta}(a_t | I, a_{<t}, o_{<t}). \quad (4)$$

where $o_{<t}$ are the tool responses seen so far. This stage aligns the model to the tool-call format, structured output tags, and basic evidence selection behavior before RL exploration begins.

Stage 3: Agentic RL. We then optimize the cold start model with GRPO [34]. For each image, the model samples multiple trajectories under the same tool environment and receives the composite reward defined in Section 3.4. The update uses group-relative advantages, which compare rollouts generated for the same image and therefore do not require a separate critic model.

$$\mathcal{L}_{\text{GRPO}}(\theta) = -\mathbb{E}_{\tau \sim \pi_{\theta}} [A(\tau) \log \pi_{\theta}(\tau | I)] + \beta_{\text{KL}} D_{\text{KL}}(\pi_{\theta} \| \pi_{\text{ref}}), \quad (5)$$

where $A(\tau) = (R(\tau) - \mu_g) / \sigma_g$, π_{ref} is the cold start reference policy, and β_{KL} keeps the policy close enough to maintain format and tool-use stability. RL follows the curriculum described above, moving from the easy subset to the full-coverage dataset.

3.4 Process reward

The reward is designed to align the model with both the final task objective and the intermediate decisions that make agentic geo-localization reliable. We decompose the trajectory reward into three terms:

$$R(\tau) = \alpha \cdot r_{\text{geo}} + \beta \cdot r_{\text{fmt}} + \gamma \cdot r_{\text{tool}}, \quad (6)$$

where hyperparameters α, β, γ control the balance between final geo-localization accuracy, strict format compliance, and intermediate tool-use quality. Default values for all reward hyperparameters are provided in Appendix C.

Geographical reward. The geographical reward r_{geo} evaluates the final predicted location. We compute the Haversine distance $d(\hat{y}, y)$ between the predicted and ground-truth coordinates, then map it to the standard geo-localization thresholds of 1, 25, 200, 750, and 2500 km. Predictions within these thresholds receive decreasing scores from street-level to continent-level accuracy, while parse failures and predictions beyond 2500 km receive zero reward.

Format reward. The format reward r_{fmt} encourages stable and interpretable trajectories. A full score is assigned when the response contains valid `<think>`, `<useful>`, and `<answer>` tags in the required format. Partial credit is given when the reasoning and final answer are valid but evidence selection is missing. Invalid formatting receives zero reward.

Tool process reward (r_{tool}). To supervise the multi-step search process, we provide per-turn rewards that are summed and clipped to prevent reward inflation from repetitive tool usage:

$$r_{\text{tool}} = \text{clip}(\sum_t r_t, -0.5, 1.0). \quad (7)$$

The turn-level reward r_t encompasses execution rewards and a discrimination reward:

- *Image search execution:* Incentivizes precise crop selection via a continuous IoU reward, $r_t^{\text{img}} = \lambda_{\text{IoU}} \cdot \text{IoU}(b_{\text{pred}}, b_{\text{gt}}) \cdot \mathbb{I}[\text{IoU} \geq \tau]$.
- *Text search execution:* Provides a fixed base reward $r_t^{\text{txt}} = \lambda_{\text{base}}$ per valid query.
- *Zoom execution:* Imposes a penalty $-\delta$ for degenerate bounding boxes.

MCC discrimination reward. A core challenge in training agents to consume search results is reward hacking: if the evaluation metric for evidence selection is strictly non-negative (e.g., Accuracy or F1 score), models rapidly learn to indiscriminately tag all retrieved results as `<useful>` to guarantee a positive reward. To prevent this, we introduce a Matthews Correlation Coefficient (MCC)-based discrimination reward. After any turn receiving search results, the model’s `<useful>` tag predictions are evaluated against the geo-informative ground truth labels. We compute MCC as:

$$\text{MCC} = \frac{\text{TP} \cdot \text{TN} - \text{FP} \cdot \text{FN}}{\sqrt{(\text{TP} + \text{FP})(\text{TP} + \text{FN})(\text{TN} + \text{FP})(\text{TN} + \text{FN})}}, \quad (8)$$

assigning the reward $r_t^{\text{mcc}} = \lambda_{\text{mcc}} \cdot \text{MCC}$. Unlike F1, MCC operates in $[-1, 1]$ and strictly penalizes both false positives and false negatives. Crucially, it evaluates to zero for constant predictors (e.g., "mark all as useful"), completely eliminating the hacking vector and forcing the model to genuinely learn *what to trust*.

4 Experiments

We evaluate REVERSE on two standard geo-localization benchmarks: Im2GPS3k [16] (2,997 geotagged images sampled worldwide) and YFCC4k [17] (4,536 images skewed toward everyday scenes with fewer prominent landmarks, making it harder). We report accuracy at 1, 25, 200, 750, and 2500 km; an unparsed prediction counts as incorrect. Baselines span classification-based methods (PlaNet, CPlaNet, ISNs, GeoToken), retrieval-based methods (GeoCLIP, Img2Loc, PIGEON), VLM-based methods (G3, GeoBayes, Geo-R), plus untuned Qwen3-VL-4B/8B as zero-shot references. REVERSE is built on Qwen3-VL-4B-Instruct and trained in three stages on 32 A800 GPUs; full hyperparameters are in Appendix D. We also conduct ablation studies on training stages, process reward components, and tool combinations.

4.1 Main results

Table 1 compares REVERSE to prior methods on Im2GPS3k and YFCC4k.

Im2GPS3k. REVERSE achieves 48.3% at 25 km and 22.5% at 1 km on Im2GPS3k, outperforming all prior methods at fine-grained thresholds. Against Geo-R [10], the strongest comparable VLM-based method, REVERSE gains 6.8 points at 25 km, from 41.5% to 48.3%. A 4B model trained with REVERSE also surpasses untuned Qwen3-VL-8B at both thresholds: 22.5% vs. 10.5% at 1 km and 48.3% vs. 37.2% at 25 km, showing that targeted training outweighs model scale. At coarser thresholds, REVERSE remains competitive but trails the strongest retrieval baselines, a gap we attribute to the near-distance bias of easy-curriculum RL that full-curriculum training partially corrects (see §4.2).

YFCC4k. On YFCC4k, REVERSE reaches 27.5% at 25 km, well above the untuned Qwen3-VL-4B baseline at 12.4%, but below retrieval-based methods such as G3 at 35.9%. YFCC4k skews toward landmark-scarce everyday scenes where image search returns generic or uninformative results. Process rewards help when tools can retrieve useful evidence, but provide little leverage when the scene offers no discriminative visual cues to begin with. This gap points to a meaningful limitation of tool-augmented approaches on visually ambiguous images.

Table 1: **Main results on Im2GPS3k and YFCC4k.** Accuracy (%) at multiple distance thresholds. Unparsed predictions count as incorrect.

Method	Venue	Im2GPS3k					YFCC4k				
		@1km	@25km	@200km	@750km	@2500km	@1km	@25km	@200km	@750km	@2500km
<i>Classification-based</i>											
kNN	ICCV'17	7.2	19.4	26.9	38.9	55.9	2.3	5.7	11.0	23.5	42.0
PlaNet	ECCV'16	8.5	24.8	34.3	48.4	64.6	5.6	14.3	22.2	36.4	55.8
CPlaNet	ECCV'18	10.2	26.5	34.6	48.6	64.6	7.9	14.8	21.9	36.4	55.5
ISNs	ECCV'18	10.5	28.0	36.6	49.7	66.0	6.5	16.2	23.8	37.4	55.0
GeoToken	ICDM'25	16.8	39.6	53.8	70.8	85.0	24.3	35.3	46.6	64.2	78.6
<i>Retrieval-based</i>											
GeoCLIP	NeurIPS'23	14.1	34.5	50.7	69.7	83.8	9.6	19.3	32.6	55.0	74.7
Img2Loc	SIGIR'24	15.3	39.8	53.6	69.7	82.8	19.8	30.7	41.4	58.1	74.1
PIGEON	CVPR'24	11.3	36.7	53.8	72.4	85.3	10.4	23.7	40.6	62.2	77.7
G3	NeurIPS'24	16.7	40.9	55.6	71.2	84.7	24.0	35.9	47.0	64.3	78.2
<i>VLM-based</i>											
Translocator	ECCV'22	11.8	31.1	46.7	58.9	80.1	8.4	18.6	27.0	41.1	60.4
GeoDecoder	ICCV'23	12.8	33.5	45.9	61.0	76.1	10.3	24.4	33.9	50.0	68.7
GeoBayes	AAAI'26	6.3	34.7	53.6	73.7	85.9	4.9	16.1	30.9	55.8	75.4
Qwen3-VL-4B	—	8.5	32.3	47.8	62.6	71.0	3.0	12.4	23.2	38.6	51.9
Qwen3-VL-8B	—	10.5	37.2	55.3	72.8	84.9	3.3	10.8	19.6	31.1	40.4
SpotAgent	KDD'26	14.1	40.4	57.8	73.4	85.8	7.3	21.5	36.2	55.0	70.8
Geo-R	AAAI'26	18.1	41.5	58.3	75.3	86.4	10.5	22.7	40.0	60.8	75.8
REVERSE (ours)	—	22.5	48.3	59.3	73.5	84.8	14.1	27.5	38.1	53.8	70.6

4.2 Ablation studies

Training pipeline stages. Table 2 traces each training stage on Im2GPS3k. The base model without tools achieves 32.3% at 25 km; adding tools without training slightly raises 25 km accuracy to 36.0% but hurts at 750 km, from 62.6% to 60.9%, confirming that tool use requires training to be effective (see also §4.3). SFT on 4M geo-tagged images raises 25 km accuracy by 10.2 points to 42.5% by building strong geographic memory before any agentic behavior is introduced. As shown in Figure 6 in Appendix F, accuracy improves throughout training with no sign of saturation, and 4B and 8B

models converge to nearly identical accuracy. Agentic Cold Start transfers these priors into the agentic format: it reaches 43.7% at 25 km, just above the SFT ceiling, but coverage drops to 90.5% as the model has not yet learned to reliably terminate. Easy-curriculum RL restores coverage to 98% and pushes 25 km to 46.2%, stabilizing tool-use termination while continuing to improve accuracy. Full-curriculum RL then trains on harder, long-range samples, recovering the 750 km and 2500 km accuracy lost during the easy phase and reaching 73.5% and 84.8% respectively.

Table 2: **Training pipeline ablation** on Im2GPS3k. Each row adds one stage on top of the previous. *Coverage*: fraction of samples producing a valid coordinate output (unparsed predictions count as incorrect in all accuracy columns). *AvgTool*: average number of tool calls per sample.

Stage	@1km	@25km	@200km	@750km	@2500km	Coverage	AvgTool
Qwen3-VL-4B (no tool)	8.5	32.3	47.8	62.6	71.0	71.3%	0.0
Qwen3-VL-4B (3 tools)	11.2	36.0	48.8	60.9	71.5	83.0%	3.9
Qwen3-VL-4B + SFT	18.1	42.5	57.6	74.8	85.9	100%	0.0
+ Agentic Cold Start	20.0	43.7	53.9	66.6	77.3	90.5%	2.7
+ Easy-curriculum RL	21.0	46.2	56.4	68.4	79.5	98.0%	3.1
+ Full-curriculum RL	22.5	48.3	59.3	73.5	84.8	99.1%	3.0

Process reward design. Table 3 ablates each component of the process reward. Removing the IoU reward leaves 25 km accuracy unchanged at 45.4%, suggesting the MCC signal already implicitly guides crop selection. Removing the MCC reward drops 25 km by 1.8 points to 43.6%, confirming that explicit evidence discrimination is needed to make accurate use of search results. Removing the search utility reward causes the largest single-component drop, 2.4 points to 43.0%, showing it is the most critical process-level signal. Removing all tool rewards reduces 25 km by 3.2 points to 42.2%, confirming that the three components collectively contribute beyond outcome-only training. Relaxing the IoU threshold from 0.7 to 0.5 hurts particularly at 750 km, from 69.8% to 66.0%, as the looser threshold admits off-target crops that introduce noisy reward signal.

Table 3: **Process reward ablation** on Im2GPS3k. All variants share the same easy-curriculum data. γ = tool reward weight in the total reward; α = accuracy reward weight.

Variant	Acc	IoU	MCC	Search	α	γ	@25km	@750km	AvgTool
Full (ours)	✓	✓	✓	✓	0.6	0.3	45.4	69.8	3.02
w/o IoU reward	✓		✓	✓	0.6	0.3	45.4	69.4	3.04
w/o MCC reward	✓	✓		✓	0.6	0.3	43.6	69.0	3.0
w/o Search reward	✓	✓	✓		0.6	0.3	43.0	68.0	3.02
Acc only	✓				1.0	0	42.2	67.8	2.90
IoU thresh 0.5	✓	✓	✓	✓	0.6	0.3	43.4	66.0	3.15

4.3 Analysis

Tool selection. Table 7 evaluates which tools contribute to accuracy using the same trained REVERSE model on Im2GPS3k. Image search is the dominant tool: used alone, it reaches the highest accuracy at most thresholds by retrieving visually similar landmarks to anchor location hypotheses. Text search adds complementary gains at fine-grained thresholds, grounding the model’s reasoning with web evidence. Combining both achieves the best balance across thresholds, and adding zoom on top yields the best overall results, consistent with the IoU reward having trained effective crop selection. Full results are in Table 7 (Appendix E).

Case study. Figure 4 shows a case where REVERSE succeeds while untuned Qwen3-VL-4B-Instruct fails. Both models receive identical image search results pointing clearly to Zuccotti Park, New York City. The untuned model rejects this evidence, reasoning that the architecture looks more like Chicago Loop, and follows a second search to the wrong city. REVERSE correctly reads the first result, identifies the sculpture as Joie de Vivre in Zuccotti Park, and uses text search to confirm coordinates before answering. The contrast illustrates the core failure mode of untuned VLMs as tool-users: strong visual priors override retrieved evidence even when the evidence is unambiguous.

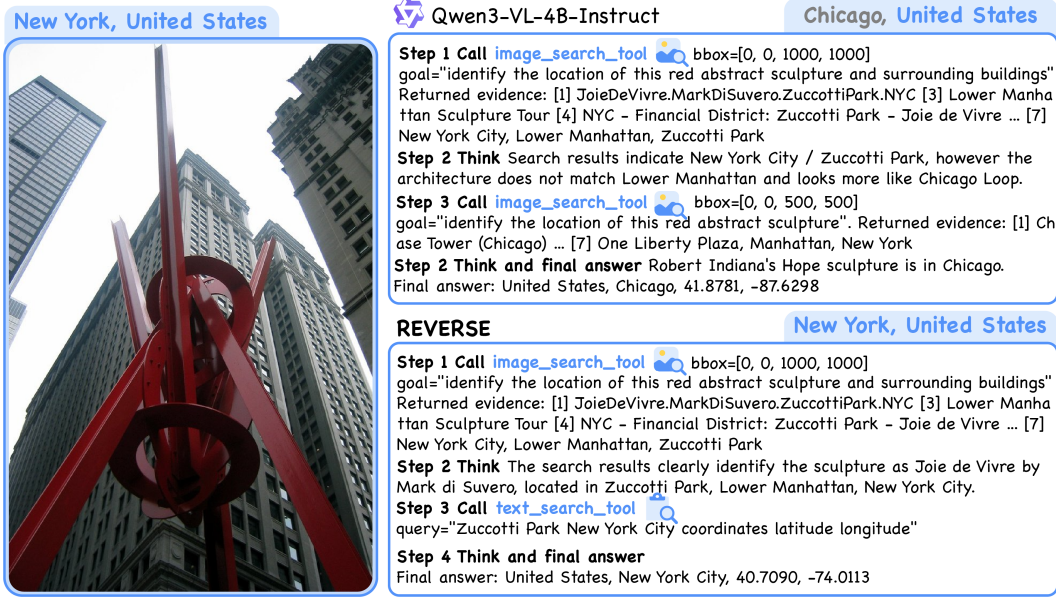


Figure 4: **Comparison of two agent trajectories on the same geo-localization case.** The Qwen3-VL-4B-Instruct trajectory first retrieves strong evidence for Joie de Vivre at Zuccotti Park, New York City, but rejects it based on a Chicago architectural prior and follows a cropped-search distractor to Chicago. **REVERSE**'s trajectory keeps the full-image evidence, identifies the sculpture as Mark di Suvero's Joie de Vivre in Zuccotti Park, and correctly predicts New York City.

RL shapes tool-use patterns, not just frequency.

Figure 5 compares per-tool invocation rates across three training stages. The untuned model over-relies on zoom at 1.53 calls per sample and invokes all three tools indiscriminately, with no apparent sense of when each is useful. Agentic Cold Start cuts zoom usage to 0.20 and shifts toward text search at 1.45, reflecting that the SFT trajectories teach the image-search to text-search reasoning chain. **REVERSE** sharpens this further: zoom nearly disappears at 0.07, image search rises to 1.56, and text search reaches 2.75 calls per sample. This progressive shift from visual-only to search-grounded reasoning is exactly the behavior our process rewards are designed to elicit, and the numbers confirm it.

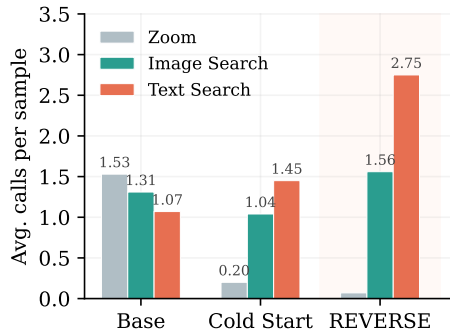


Figure 5: **Tool calls per sample** across training stages on Im2GPS3k. Base: untuned Qwen3-VL-4B. Cold Start: Stage 2. **REVERSE**: full-curriculum RL.

5 Conclusion

This paper addresses image geo-localization by recasting it as an active, multi-turn reasoning process. The key idea is that a model should learn to inspect regions, retrieve external evidence, and judge what to trust, rather than committing to a single prediction from one forward pass. We train a 4B VLM with zoom and search tools via GRPO, supervised by process-level rewards that cover where to search, how to query, and what to believe. On Im2GPS3k, **REVERSE** reaches 48.3% at 25 km, outperforming prior VLM-based methods and surpassing the untuned 8B baseline despite using a model half its size. A core finding is that tool use must be trained, not just enabled: equipping untuned models with tools hurts accuracy, while process rewards teach the model to use tools selectively and interpret their results critically.

References

- [1] Gengchen Mai, Weiming Huang, Jin Sun, Suhang Song, Deepak Mishra, Ninghao Liu, Song Gao, Tianming Liu, Gao Cong, Yingjie Hu, Chris Cundy, Ziyuan Li, Rui Zhu, and Ni Lao. On the opportunities and challenges of foundation models for GeoAI. *ACM Transactions on Spatial Algorithms and Systems*, 10(2):1–46, 2024.
- [2] Guillaume Astruc, Nicolas Dufour, Ioannis Siglidis, Constantin Aronssohn, Nacim Bouia, Stephanie Fu, Romain Loiseau, Van Nguyen Nguyen, Charles Raude, Elliot Vincent, Lintao Xu, Hongyu Zhou, and Loic Landrieu. OpenStreetView-5M: The many roads to global visual geolocation. In *Proceedings of the IEEE/CVF Conference on Computer Vision and Pattern Recognition*, pages 21967–21977, 2024.
- [3] Tobias Weyand, Ilya Kostrikov, and James Philbin. PlaNet - photo geolocation with convolutional neural networks. In *European Conference on Computer Vision (ECCV)*, 2016.
- [4] Paul Hongsuck Seo, Tobias Weyand, Jack Sim, and Bohyung Han. CPlaNet: Enhancing image geolocalization by combinatorial partitioning of maps. In *European Conference on Computer Vision (ECCV)*, 2018.
- [5] Eric Müller-Budack, Kader Pustu-Iren, and Ralph Ewerth. Geolocation estimation of photos using a hierarchical model and scene classification. In *European Conference on Computer Vision (ECCV)*, 2018.
- [6] V. Vivanco Cepeda, Gaurav Kumar Nayak, and Mubarak Shah. GeoCLIP: Clip-inspired alignment between locations and images for effective worldwide geo-localization. In *Advances in Neural Information Processing Systems (NeurIPS)*, 2023.
- [7] Lukas Haas, Michal Skreta, Silas Alberti, and Chelsea Finn. PIGEON: Predicting image geolocations. In *IEEE/CVF Conference on Computer Vision and Pattern Recognition (CVPR)*, 2024.
- [8] Zhongliang Zhou, Jieli Zhang, Zihan Guan, Jiayu Hu, Shuwei Lao, Kaiye Mu, Yunqi Li, and Gengchen Mai. Img2Loc: Revisiting image geolocalization using multi-modality foundation models and image-based retrieval-augmented generation. In *Proceedings of the 47th International ACM SIGIR Conference on Research and Development in Information Retrieval (SIGIR)*, 2024.
- [9] Pengyue Jia, Yiding Liu, Xiaopeng Li, Yuhao Wang, Yantong Du, Xiao Han, Xuetao Wei, Shuaiqiang Wang, Dawei Yin, and Xiangyu Zhao. G3: An effective and adaptive framework for worldwide geolocalization using large multi-modality models. In *Advances in Neural Information Processing Systems (NeurIPS)*, 2024.
- [10] Biao Wu, Meng Fang, Ling Chen, Ke Xu, Tao Cheng, and Jun Wang. Vision-language reasoning for geolocalization: A reinforcement learning approach. In *Proceedings of the AAAI Conference on Artificial Intelligence (AAAI)*, 2026.
- [11] Modi Jin, Yiming Zhang, Boyuan Sun, Dingwen Zhang, MingMing Cheng, and Qibin Hou. Geoagent: Learning to geolocate everywhere with reinforced geographic characteristics. *arXiv preprint arXiv:2602.12617*, 2026.
- [12] Furong Jia, Ling Dai, Wenjin Deng, Fan Zhang, Chen Hu, Daxin Jiang, and Yu Liu. Spotagent: Grounding visual geo-localization in large vision-language models through agentic reasoning. *arXiv preprint arXiv:2602.09463*, 2026.
- [13] Yuxiang Ji, Yong Wang, Ziyu Ma, Yiming Hu, Hailang Huang, Xuecai Hu, Guanhua Chen, Liaoni Wu, and Xiangxiang Chu. Thinking with map: Reinforced parallel map-augmented agent for geolocalization. *arXiv preprint arXiv:2601.05432*, 2026.
- [14] Xiao Han, Chen Zhu, Xiangyu Zhao, and Hengshu Zhu. Swarm intelligence in geo-localization: A multi-agent large vision-language model collaborative framework. In *Proceedings of the 31st ACM SIGKDD Conference on Knowledge Discovery and Data Mining V. 2*, pages 814–825, 2025.

- [15] Yikun Wang, Zuyan Liu, Ziyi Wang, Han Hu, Pengfei Liu, and Yongming Rao. GeoVista: Web-augmented agentic visual reasoning for geolocalization. *arXiv preprint arXiv:2511.15705*, 2025.
- [16] Nam Vo, Nathan Jacobs, and James Hays. Revisiting IM2GPS in the deep learning era. In *IEEE International Conference on Computer Vision (ICCV)*, 2017.
- [17] Bart Thomee, David A. Shamma, Gerald Friedland, Benjamin Elizalde, Karl Ni, Douglas Poland, Damian Borth, and Li-Jia Li. YFCC100M: The new data in multimedia research. In *Communications of the ACM*, 2016.
- [18] Shraman Pramanick, Ewa M. Nowara, Joshua Gleason, Carlos D. Castillo, and Rama Chellappa. Where in the world is this image? Transformer-based geo-localization in the wild. In *European Conference on Computer Vision (ECCV)*, 2022.
- [19] Brandon Clark, Alec Kerrigan, Parth Parag Kulkarni, Vicente Vivanco Cepeda, and Mubarak Shah. Where we are and what we’re looking at: Query based worldwide image geo-localization using hierarchies and scenes. In *Proceedings of the IEEE/CVF Conference on Computer Vision and Pattern Recognition*, pages 23182–23190, 2023.
- [20] Pengyue Jia, Seongheon Park, Song Gao, Xiangyu Zhao, and Sharon Li. GeoRanker: Distance-aware ranking for worldwide image geolocalization. In *Advances in Neural Information Processing Systems (NeurIPS)*, 2025.
- [21] Ling Li, Yao Zhou, Yuxuan Liang, Fugee Tsung, and Jiaheng Wei. Recognition through reasoning: Reinforcing image geo-localization with large vision-language models. *arXiv preprint arXiv:2506.14674*, 2025.
- [22] Shunyu Yao, Jeffrey Zhao, Dian Yu, Nan Du, Izhak Shafran, Karthik Narasimhan, and Yuan Cao. React: Synergizing reasoning and acting in language models. *arXiv preprint arXiv:2210.03629*, 2022.
- [23] Timo Schick, Jane Dwivedi-Yu, Roberto Dessì, Roberta Raileanu, Maria Lomeli, Eric Hambro, Luke Zettlemoyer, Nicola Cancedda, and Thomas Scialom. Toolformer: Language models can teach themselves to use tools. *Advances in neural information processing systems*, 36: 68539–68551, 2023.
- [24] Dídac Surís, Sachit Menon, and Carl Vondrick. Vipergpt: Visual inference via python execution for reasoning. In *Proceedings of the IEEE/CVF international conference on computer vision*, pages 11888–11898, 2023.
- [25] Zhengyuan Yang, Linjie Li, Jianfeng Wang, Kevin Lin, Ehsan Azarnasab, Faisal Ahmed, Zicheng Liu, Ce Liu, Michael Zeng, and Lijuan Wang. Mm-react: Prompting chatgpt for multimodal reasoning and action. *arXiv preprint arXiv:2303.11381*, 2023.
- [26] Penghao Wu and Saining Xie. V?: Guided visual search as a core mechanism in multimodal llms. In *Proceedings of the IEEE/CVF Conference on Computer Vision and Pattern Recognition*, pages 13084–13094, 2024.
- [27] Jack Hong, Chenxiao Zhao, ChengLin Zhu, Weiheng Lu, Guohai Xu, and Xing Yu. Deepeyesv2: Toward agentic multimodal model. *arXiv preprint arXiv:2511.05271*, 2025.
- [28] Wenxuan Huang, Yu Zeng, Qiuchen Wang, Zhen Fang, Shaosheng Cao, Zheng Chu, Qingyu Yin, Shuang Chen, Zhenfei Yin, Lin Chen, Zehui Chen, Xu Tang, Yao Hu, Shaohui Lin, Philip Torr, Feng Zhao, and Wanli Ouyang. Vision-deepresearch: Incentivizing deepresearch capability in multimodal large language models. *arXiv preprint arXiv:2601.22060*, 2026.
- [29] Yu Zeng, Wenxuan Huang, Zhen Fang, Shuang Chen, Yufan Shen, Yishuo Cai, Xiaoman Wang, Zhenfei Yin, Lin Chen, Zehui Chen, Shiting Huang, Yiming Zhao, Xu Tang, Yao Hu, Philip Torr, Wanli Ouyang, and Shaosheng Cao. Vision-deepresearch benchmark: Rethinking visual and textual search for multimodal large language models. *arXiv preprint arXiv:2602.02185*, 2026.

- [30] Zeyi Huang, Yuyang Ji, Anirudh Sundara Rajan, Zefan Cai, Wen Xiao, Haohan Wang, Junjie Hu, and Yong Jae Lee. Visualtoolagent (vista): A reinforcement learning framework for visual tool selection. *arXiv preprint arXiv:2505.20289*, 2025.
- [31] Qihua Dong, Gozde Sahin, Pei Wang, Zhaowei Cai, Robik Shrestha, Hao Yang, and Davide Modolo. Visual reasoning through tool-supervised reinforcement learning. *arXiv preprint arXiv:2604.19945*, 2026.
- [32] Xintong Zhang, Zhi Gao, Bofei Zhang, Pengxiang Li, Xiaowen Zhang, Yang Liu, Tao Yuan, Yuwei Wu, Yunde Jia, Song-Chun Zhu, and Qing Li. Chain-of-focus: Adaptive visual search and zooming for multimodal reasoning via rl. *arXiv e-prints*, pages arXiv–2505, 2025.
- [33] Shuai Bai, Yuxuan Cai, Ruizhe Chen, Keqin Chen, Xionghui Chen, Zesen Cheng, Lianghao Deng, Wei Ding, Chang Gao, Chunjiang Ge, Wenbin Ge, Zhifang Guo, Qidong Huang, Jie Huang, Fei Huang, Binyuan Hui, Shutong Jiang, Zhaohai Li, Mingsheng Li, Mei Li, Kaixin Li, Zicheng Lin, Junyang Lin, Xuejing Liu, Jiawei Liu, Chenglong Liu, Yang Liu, Dayiheng Liu, Shixuan Liu, Dunjie Lu, Ruilin Luo, Chenxu Lv, Rui Men, Lingchen Meng, Xuancheng Ren, Xingzhang Ren, Sibao Song, Yuchong Sun, Jun Tang, Jianhong Tu, Jianqiang Wan, Peng Wang, Pengfei Wang, Qiuyue Wang, Yuxuan Wang, Tianbao Xie, Yiheng Xu, Haiyang Xu, Jin Xu, Zhibo Yang, Mingkun Yang, Jianxin Yang, An Yang, Bowen Yu, Fei Zhang, Hang Zhang, Xi Zhang, Bo Zheng, Humen Zhong, Jingren Zhou, Fan Zhou, Jing Zhou, Yuanzhi Zhu, and Ke Zhu. Qwen3-VL technical report. *arXiv preprint arXiv:2511.21631*, 2025.
- [34] Zhihong Shao, Peiyi Wang, Qihao Zhu, Runxin Xu, Junxiao Song, Xiao Bi, Haowei Zhang, Mingchuan Zhang, Y.K. Li, Y. Wu, and Daya Guo. DeepSeekMath: Pushing the limits of mathematical reasoning in open language models. *arXiv preprint arXiv:2402.03300*, 2024.
- [35] Narges Ghasemi, Amir Ziashahabi, Salman Avestimehr, and Cyrus Shahabi. GeoToken: Hierarchical geolocalization of images via next token prediction. In *IEEE International Conference on Data Mining (ICDM)*, 2025.
- [36] Brandon Clark, Alec Kerrigan, Parth Parag Kulkarni, Vicente Vivanco Cepeda, and Mubarak Shah. Where we are and what we’re looking at: Query based worldwide image geo-localization using hierarchies and scenes. In *IEEE/CVF International Conference on Computer Vision (ICCV)*, 2023.
- [37] Weimin Shi, Xiang Li, Kaige Li, Junhao Fang, Qiang Zhou, Qichuan Geng, and Zhong Zhou. GeoBayes: Probabilistic image geo-localization inference via sequential bayesian updating. In *Proceedings of the AAAI Conference on Artificial Intelligence (AAAI)*, 2026.
- [38] Guangming Sheng, Chi Zhang, Zilingfeng Ye, Xibin Wu, Wang Zhang, Ru Zhang, Yanghua Peng, Haibin Lin, and Chuan Wu. HybridFlow: A flexible and efficient RLHF framework. *arXiv preprint arXiv:2409.19256*, 2024.
- [39] Lianmin Zheng, Liangsheng Yin, Zhiqiang Xie, Chuyue Sun, Jeff Huang, Cody Hao Yu, Shiyi Cao, Christos Kozyrakis, Ion Stoica, Joseph E. Gonzalez, Clark Barrett, and Ying Sheng. SGLang: Efficient execution of structured language model programs. *arXiv preprint arXiv:2312.07104*, 2023.

A Agent Implementation Details

A.1 Prompt

To ensure consistency between training and evaluation, we adopt a unified prompt template used verbatim during both Agentic Cold Start and RL rollout. The template is designed to guide the model through systematic visual reasoning of geographic clues while enforcing a *think-then-act* pattern for tool use: the model must always reason in `<think>` before issuing any tool call or final answer. Beyond standard tool-use instructions, our prompt introduces two REVERSE-specific mechanisms: (i) explicit **decision rules** that govern which tool to call given the visual context (e.g., image search for landmarks, zoom for small text), and (ii) an **evidence discrimination** tag `<useful>` that forces the model to identify which retrieved results are geographically relevant to the specific image—this tag directly drives our MCC process reward during RL training.

A.2 Example Inference Trace

The trace below shows a complete two-turn inference from REVERSE on a real Im2GPS3k image (id: 311938754, prediction error: 3.4 km). The model identifies a distinctive astronomical instrument via image search, discriminates the relevant results with `<useful>`, and confirms the exact coordinates through a follow-up text search before issuing its final answer.

A.3 Agent Tool Infrastructure

REVERSE exposes three tools to the agent at inference time. All tool calls are formatted as structured JSON inside `<tool_call> . . . </tool_call>` tags, following the same format used during Agentic Cold Start training.

Image Zoom Tool. The zoom tool implements a deterministic crop-and-resize pipeline. Given normalized bounding-box coordinates $[x_1, y_1, x_2, y_2]$ in $[0, 1000]^2$, the tool maps them to pixel-level crops via linear scaling to the image dimensions. The crop is then resized following Qwen3-VL’s `smart_resize` scheme: output resolution is snapped to multiples of the patch factor (28 pixels), with a minimum of 256×256 and a maximum of 2048×1024 pixels, preserving aspect ratio. The resized crop is re-injected into the model’s context as a new image token sequence, allowing fine-grained inspection of text, inscriptions, or small visual details not visible at full scale.

Image Search Tool. The reverse image search tool crops the specified region using the same pipeline as the zoom tool, uploads the crop to cloud object storage to obtain a public URL, and queries the Oxy Labs Google Lens API. Results are returned as a ranked list of up to 10 web pages, each containing a title, source URL, and domain. The agent marks useful results with `<useful>[. . .]</useful>` tags, which serve as the discrimination signal for the MCC reward during RL training.

Web Search Tool. The text search tool submits natural-language queries to the Tavily Search API, returning up to 5 results per query with titles, snippets, and source URLs. The tool supports parallel multi-query execution: if the agent provides a list of queries, all are dispatched concurrently and results are concatenated. API keys are managed via a pool with automatic rotation on quota exhaustion. Both image search and text search results are cached in a local SQLite database (WAL mode) to ensure reproducibility across evaluation runs.

A.4 Offline Search Cache for RL Rollout

Live API calls during RL rollout are expensive and non-reproducible. We pre-annotate the training corpus with tool call–response pairs offline and cache them in a Parquet-based lookup table keyed by (image hash, bounding box) for image search and by query string for text search. During rollout, cache hits are served instantly; cache misses fall back to live API calls. This hybrid strategy reduces API cost by over 90% while retaining full coverage for novel queries generated by the evolving policy.

Prompt Template

You are a geolocation expert. Given an image, identify its location.

Available Tools

The agent can invoke the following tools:

- **image_search_tool**: Reverse image search using a cropped region. Best for distinctive landmarks, buildings, or scenes. Returns matching web pages.
 - *Parameters*: `bbox_2d [x1, y1, x2, y2]` — crop region; `goal` — description of what to identify.
- **text_search_tool**: Search the web with natural language queries. Use for visible text/signs, landmark names, or any clues found from image search results. Supports a list of parallel queries.
 - *Parameters*: `query` — a string or list of search strings.
- **image_zoom_in_tool**: Zoom into a region to read text or inscriptions that are too small at full scale.
 - *Parameters*: `bbox_2d [x1, y1, x2, y2]` — region to zoom.

Decision Rules

- Distinctive landmark or scene visible (but uncertain of exact coords) → use **image_search_tool**.
- Text/signs already legible → use **text_search_tool** directly.
- Text/signs too small to read → use **image_zoom_in_tool** first, then **text_search_tool**.
- Image search returns a landmark/location name → follow up with **text_search_tool**.
- Do **not** use **image_zoom_in_tool** before **image_search_tool** — zoom does not improve image search.
- When in doubt, use a tool. Only skip tools when certain.
- **Fallback rule**: If tools have failed, returned empty results, or exceeded call limits, do **not** keep retrying. Provide your best `<answer>` based on visual priors. Never finish a response without a `<tool_call>` or `<answer>`.

Reasoning Requirement

For every response, first enclose your reasoning in `<think> ... </think>` tags, then output **exactly one** of:

```
<tool_call>{"name": "image_search_tool", "arguments": {"bbox_2d": [x1,y1,x2,y2], "goal": "..."}}</tool_call>
<tool_call>{"name": "text_search_tool", "arguments": {"query": "..."}}</tool_call>
<tool_call>{"name": "text_search_tool", "arguments": {"query": ["q1","q2"]}}</tool_call>
<tool_call>{"name": "image_zoom_in_tool", "arguments": {"bbox_2d": [x1,y1,x2,y2]}}</tool_call>
```

or your final `<answer>` when confident without needing a tool.

Evidence Discrimination

After receiving tool results, output on its own line: `<useful>[i, j, ...]</useful>` listing the 1-based indices of results that match this specific image. Results about a different place are **not** useful even if they contain geographic information. Output `<useful>[]</useful>` if none match.

Final Answer Format

When ready to answer, provide the final answer inside `<answer> ... </answer>` tags. The final answer must include Country, City, Latitude, and Longitude (decimal format).

Example: `<answer>Italy, Golfo Arnaci, 40.9606, 9.5873</answer>`

Latitude and longitude must always be valid numeric values and cannot be null.

User: *[Image: circular hemispherical astronomical instrument, stone construction, Jaipur, India]*

Assistant (Turn 1):

<think> The image shows a circular structure with a reflective surface, appearing to be a sundial or astronomical instrument. This is a distinctive landmark. Let me run image search to identify it. </think>
 <tool_call>{"name": "image_search_tool", "arguments": {"bbox_2d": [0, 0, 1000, 1000], "goal": "identify this circular astronomical instrument"}}</tool_call>

Tool Response (image_search_tool):

- [1] File:JaiPrakashYantraJaipur20080213-1.jpg — Wikimedia Commons
- [2] Jai Prakash Yantra, measuring time through a hemispherical. . . — traveladventures.org
- [3] Jantar Mantar, Jaipur — Wikipedia
- [4] Detail of the Jai Prakash Yantra, a sundial which measures. . . — Alamy
- [5] Jantar Mantar Observatory — markandchucksadventures.com
- [6] File:Zodiac Circle jantar mantar, Jaipur 1.jpg — Wikimedia Commons
- [7] Jantar Mantar: Jaipur's Famous Observatory — throughmylens.com
- [8] Jai Prakash Yantra Jantarantar Observatory — Tripadvisor
- [9] Under Jaipur Skies: Jantar Mantar — shaopeng.blog
- [10] 617 Sundial Jantar Mantar Jaipur Stock Photos — Dreamstime.com

Assistant (Turn 2):

<think> The results clearly identify this as the Jai Prakash Yantra at Jantar Mantar Observatory in Jaipur, Rajasthan, India. Let me confirm the exact coordinates with a text search. </think>
 <useful>[1, 2, 3, 4, 5]</useful>
 <tool_call>{"name": "text_search_tool", "arguments": {"query": "Jantar Mantar Observatory Jaipur coordinates latitude longitude"}}</tool_call>

Tool Response (text_search_tool):

- [1] GPS coordinates of Jantar Mantar (Jaipur), India. Latitude: 26.9215, Longitude: 75.8213 — latitude.to
 The Jantar Mantar monument of Jaipur is a collection of nineteen astronomical instruments built by the Rajput king Sawai Jai Singh, completed in 1738 CE. Latitude: 26°55'17.39"N, Longitude: 75°49'16.79"E. Nearest city: Jaipur.
- [2] Jantar Mantar, Jaipur — Wikipedia
 Kranti Vriitta Yantra (measures longitude and latitude of celestial bodies). . . Its face is angled at 27 degrees, the latitude of Jaipur.
- [3] Jantar Mantar Jaipur India — tourhq.com
 The Jantar Mantar features the world's largest stone sundial and is a UNESCO World Heritage site.
- [4] Jantar Mantar — banbanjara.com
 Sawai Jai Singh II constructed the astronomical observatory in Jaipur. 19 astrological and architectural instruments including the Vrihat Samrat Yantra.
- [5] UNESCO Portal to the Heritage of Astronomy
 The Jantar Mantar of Jaipur is an observatory built in the first half of the 18th century. One of the most complete collections of pre-telescopic masonry instruments in the world.

Assistant (Final Answer):

<think> Confirmed: Jantar Mantar Observatory, Jaipur, India. Coordinates 26.9215°N, 75.8213°E from the first result. </think>
 <useful>[1]</useful>
 <answer>India, Jaipur, 26.9215, 75.8213</answer>

B Training Data Construction

Our training corpora are built from oracle-generated trajectories using Kimi-K2.6 as the annotation agent. We randomly sample 100K images from MP16-Pro and prompt Kimi-K2.6 to solve each using the same agentic tool interface as REVERSE, without revealing the ground-truth location. This yields ~30,750 valid raw trajectories after discarding failed or inaccessible cases. The remaining MP16-Pro images (approximately 4M) are used for Stage 1 SFT as coordinate-only supervision. We apply a cascade of quality filters to the 30,750 trajectories to produce training splits of varying strictness (Table 4).

Trajectory filtering. *RL base* (19,962 trajectories): retain samples where the image is accessible, the oracle’s localization error $d \leq 200$ km, at least one tool was invoked, the trajectory did not exceed the maximum turn budget, and no tool call returned an API failure response. This is the broadest usable set and forms the basis for all downstream splits.

Agentic Cold Start (4,427 trajectories, subset of RL base): additionally require at most 5 tool calls per trajectory. This stricter constraint keeps only the most concise, self-consistent reasoning paths for supervised fine-tuning.

RL full-coverage (6,996 trajectories, subset of RL base): retain samples where every image-search call in the trajectory has been annotated with geo-informative and non-informative result labels, and at least one positive result exists per search call. This annotation is required so that the MCC discrimination reward r_t^{mcc} can be computed for every tool call during RL training. Trajectories with no search calls are also included.

Easy-curriculum subset (3,104 trajectories, subset of RL full-coverage): further restrict to $d \leq 25$ km to form the first-stage RL curriculum, focusing training on geographically unambiguous scenes before progressing to harder long-range samples.

Offline cache construction. The image search cache contains 273K entries indexed by (image path, call index). Each entry stores the oracle’s annotated bounding box, all geo-informative (positive) results, and all non-informative (negative) results from the same search call. During RL rollout, a model-generated bounding box is matched to a cache entry if $\text{IoU}(b_{\text{pred}}, b_{\text{gt}}) \geq \tau$; otherwise the tool returns an empty result, penalizing imprecise crops. The text search cache contains 82K entries indexed by a normalized query hash, matched at rollout time by token-level Jaccard similarity. Both caches cover all training and validation images, enabling fully offline RL training with no live API calls.

Table 4: Dataset statistics for Agentic Cold Start and RL training.

Split	Samples	Filter criteria
Agentic Cold Start	4,427	$d \leq 200$ km, ≤ 5 tool calls
RL easy-curriculum	3,104	full-coverage + $d \leq 25$ km
RL full-curriculum	6,996	full-coverage, ≥ 1 positive result per search call

C Training Hyperparameters

Table 5 summarizes the hyperparameters for all three training stages. REVERSE follows a progressive training schedule: Stage 1 establishes broad geographic priors via large-scale supervised learning; Stage 2 fine-tunes the model on agentic tool-use trajectories at a lower learning rate; Stage 3 applies GRPO-based RL with a two-phase curriculum, starting from easy samples ($d \leq 25$ km) before expanding to the full difficulty range.

D Experimental Setup

Benchmarks. We evaluate on two standard geolocation benchmarks. *Im2GPS3k* [16] contains 2,997 geotagged images sampled worldwide, covering diverse geographic regions and landmark types. *YFCC4k* [17] contains 4,536 images from the YFCC100M dataset and skews toward everyday scenes with fewer prominent landmarks, making it harder than Im2GPS3k. Following standard practice, accuracy at threshold r counts a prediction as correct if its Haversine distance to ground truth is within r km; unparsed predictions count as incorrect. We report accuracy at 1, 25, 200, 750, and 2500 km.

Baselines. We compare against a broad range of prior geolocation methods. *Classification-based* methods partition the Earth into geographic cells and train classifiers: PlaNet [3], CPLaNet [4], ISNs [5], kNN [16], and GeoToken [35]. *Retrieval-based* methods match query images against geo-tagged databases: GeoCLIP [6], Img2Loc [8], and PIGEON [7]. *VLM-based* methods leverage pretrained vision-language models with geographic supervision: Translocator [18], GeoDecoder [36], G3 [9], and GeoBayes [37]. We additionally evaluate Qwen3-VL-4B and Qwen3-VL-8B [33] without

Table 5: Training hyperparameters for all three stages of REVERSE.

Hyperparameter	Stage 1 (SFT)	Stage 2 (Agentic Cold Start)	Stage 3 (Agentic RL)
Base model	Qwen3-VL-4B-Instruct	Stage 1 checkpoint	Stage 2 checkpoint
Training framework	FSDP	FSDP	VERL + GRPO
Rollout engine	—	—	SGLang
Nodes (\times 8 GPUs)	8	1	4
Training data	MP16-Pro (4M)	Cold-start V5.2 (4,427)	Easy (3,104) \rightarrow Full (6,996)
Batch size	512	128	256
Learning rate	2×10^{-5}	2×10^{-5}	1×10^{-6}
LR schedule	cosine	cosine	cosine
Warmup ratio	0.1	0.1	0.05
Min-LR ratio	—	—	0.1
Training steps	\approx 7,800	35	80 (easy) + 135 (full)
Reward weights	—	—	$\alpha=0.6, \beta=0.1, \gamma=0.3$
IoU reward coeff	—	—	0.2
MCC reward coeff	—	—	0.3
Base search reward	—	—	0.1
IoU threshold	—	—	0.7
Max turns (rollout)	—	—	10
Max response length	—	—	16,384 tokens
Hardware	8 \times NVIDIA A800 80 GB per node		

Table 6: Reward hyperparameters and their default values.

Symbol	Meaning	Default
α	Geolocation reward weight	0.6
β	Format reward weight	0.1
γ	Tool reward weight	0.3
τ	IoU gate threshold	0.7
λ_{iou}	Image search IoU coeff	0.2
λ_{base}	Text search base reward	0.1
λ_{mcc}	MCC discrimination coeff	0.3
δ	Zoom invalid-box penalty	0.05

any geographic fine-tuning as untuned VLM baselines. *RL-based* methods optimize geographic reasoning with reinforcement learning: Geo-R [10].

Implementation details. REVERSE is built on Qwen3-VL-4B-Instruct [33] and trained in three stages (full hyperparameters in Table 5). **Stage 1 (SFT):** We fine-tune on 4M geo-tagged images from MP16-Pro [9] for \approx 7,800 steps on 8 nodes with batch size 512 and learning rate 2×10^{-5} . **Stage 2 (Agentic Cold Start):** We fine-tune on 4,427 curated teacher trajectories for 35 steps on 1 node with batch size 128 and learning rate 2×10^{-5} . **Stage 3 (Agentic RL):** We apply GRPO [34] with a two-phase curriculum: 80 steps on 3,104 easy samples ($d \leq 25$ km) followed by 135 steps on 6,996 full-coverage samples, using learning rate 1×10^{-6} and reward weights $\alpha=0.6, \beta=0.1, \gamma=0.3$. RL rollout uses VERL [38] and SGLang [39]. All training runs on NVIDIA A800 80 GB GPUs (8 GPUs per node).

E Tool Combination Results

F SFT Scaling

Figure 6 shows the accuracy of Qwen3-VL-4B and Qwen3-VL-8B on Im2GPS3k as a function of training samples seen during SFT (Stage 1). In this stage, the model is trained to directly output coordinates without any intermediate reasoning or tool use, purely consolidating geographic visual memory. Both models improve consistently across all distance thresholds with no sign of saturation at 4M samples. Notably, 4B and 8B converge to nearly identical accuracy, with 8B providing only marginal gains (<1 pp at @25km), motivating our choice of the 4B model.

Table 7: **Tool combination ablation** on Im2GPS3k. All variants use the same REVERSE model (full-curriculum RL). Unparsed predictions count as incorrect.

Tools	@1km	@25km	@200km	@750km	@2500km
No tool	8.5	32.3	47.8	62.6	71.0
Zoom only	12.0	38.0	58.0	64.0	84.0
Image search only	20.0	48.0	64.0	72.0	76.0
Text search only	14.0	42.0	54.0	64.0	76.0
Zoom + text search	12.0	38.0	58.0	68.0	76.0
Image + text search	22.0	47.0	58.0	72.0	80.0
Image + text + zoom	22.5	48.3	59.3	73.5	84.8

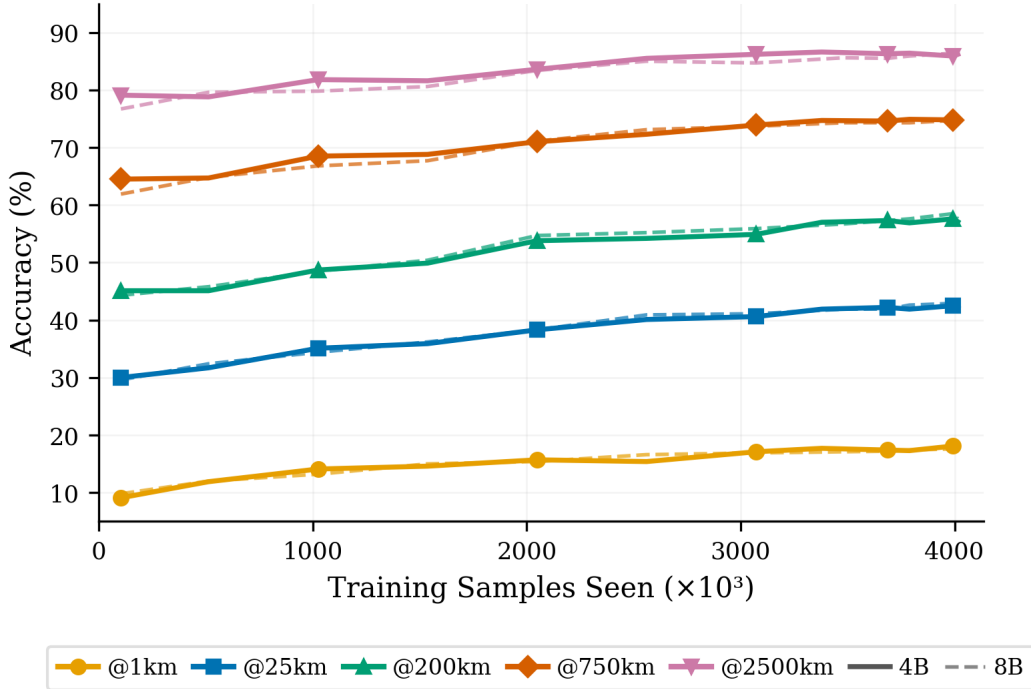


Figure 6: **SFT scaling curves** on Im2GPS3k (2,997 images). Accuracy at five distance thresholds as a function of training samples seen. Solid lines: Qwen3-VL-4B; dashed lines: Qwen3-VL-8B.

G Limitations and Broader Impacts

REVERSE trades live retrieval for reproducibility: RL training uses a static offline cache, which enables high-throughput training and controlled evaluation but means the model learns search behaviors against a fixed snapshot rather than a shifting live web. Similarly, agentic cold-start trajectories come from Kimi-K2.6; while this provides high-quality supervision, it introduces a dependency on a large proprietary teacher. We also note that our image search tool does not filter domains that expose GPS metadata such as Flickr, so retrieved results could in principle contain ground-truth coordinates. We did not observe leakage artifacts, but explicit domain filtering is a straightforward improvement for future work.

Accurate geolocation agents raise privacy concerns: they could identify individuals or sensitive locations from casually shared photographs. REVERSE is a research system exploring spatial reasoning and multi-turn tool use, and real-world deployment should include safeguards such as metadata stripping and blurring of faces and private spaces.